*Journal of Applied Fluid Mechanics*, Vol. 9, No. 5, pp. 2515-2525, 2016.
Available online at www.jafmonline.net, ISSN 1735-3572, EISSN 1735-3645.
DOI: 10.18869/acadpub.jafm.68.236.24409

# MHD Natural Convection in a Square Enclosure using Nanofluid with the Influence of Thermal Boundary Conditions

M. A. Mansour[1†], S. E. Ahmed[2†] and A. M. Rashad[3]

[1]*Department of Mathematics, Assuit University, Faculty of Science, Assuit, Egypt.*
[2]*Department of Mathematics, South Valley University, Faculty of Science, Qena, Egypt.*
[3]*Department of Mathematics, Aswan University, Faculty of Science, Aswan, Egypt.*

†*Corresponding Author Email:sameh_sci_math@yahoo.com*

(Received December 23, 2014; accepted November 2, 2015)

## ABSTRACT

Numerical investigation for heat transfer with steady MHD natural convection cooling of a localized heat source at the bottom wall of an enclosure filled with nanofluids subjected to changeable thermal boundary conditions at the sidewalls has been studied in the a presence of inclined magnetic field. Finite difference method was employed to solve the dimensionless governing equations of the problem. The effects of governing parameters, namely, Hartmann number, solid volume fraction, the different values of the heat source length and the different locations of the heat source on the streamlines and isotherms contours as well as maximum temperature, Nusselt number and average Nusselt number along the heat source were considered. The present results are validated by favorable comparisons with previously published results. The results of the problem are presented in graphical and tabular forms and discussed. It is found that an increase in the Hartmann number results in a clear reduction in the rate of heat transfer; however, the increase in Rayleigh number enhances the nanofluid flow and heat transfer rate.

**Keywords**: Magnetohydrodynamics; Natural convection; Square enclosure; Configurations; Nanofluid.

## NOMENCLATURE

| | |
|---|---|
| B | magnetic field strength |
| $C_p$ | heat capacity |
| g | gravity acceleration |
| H | height of the cavity |
| Ha | Hartmann number |
| k | thermal conductivity |
| Nu | Nusselt number |
| p | dimensional pressure |
| P | dimensionless pressure |
| Pr | Prandt lnumber |
| $q''$ | heat generation per area |
| Ra | Rayleighnumber |
| T | dimensional temperature |
| (u, v) | dimensional velocity components |
| (U, V) | dimensionless velocity components |
| (x,y) | cartesian coordinates |
| (X, Y) | dimensionless coordinates |
| α | thermal diffusivity |
| β | thermal expansion coefficient, |
| ϕ | solid volume fraction |
| θ | dimensionless temperature |
| σ | electrical conductivity |
| μ | dynamic viscosity |
| ν | kinematic viscosity |
| ρ | density |
| Φ | magnetic field inclination angle |
| ζ | ratio of nanolayer thickness to nanoparticle Radius |

**SUBSCRIPTS**

| | |
|---|---|
| c | cold wall |
| f | fluid |
| nf | nanofluid |
| p | particle |

## 1. INTRODUCTION

Nanofluids are the fluids with these nanoelements (nanoparticles, nanotubes or nanofibers) suspended in them. These fluids enhance thermal conductivity of the base fluid enormously, which is beyond the explanation of any existing theory. They are also very stable and have no additional

problems, such as sedimentation, erosion, additional pressure drop and non-Newtonian behavior, due to the tiny size of nanoelements and the low volume fraction of nanoelements required for conductivity enhancement. These, with their various potential applications, have recently attracted intensive studies on nanofluids (Choi (1995), Eastman *et al*. (2001), Xie *et al*. (2003), Jana *et al*. (2007)). Nanotechnology has been widely used in industry since materials with sizes of nanometer possess unique physical and chemical properties. Nano-scale particle added fluids are called as nanofluid which is firstly introduced by Choi (1995). Khanafer *et al*. (2003) presented study of natural convection of Copper-water nanofluid in a two dimensional rectangular enclosure. They reported an increase in heat transfer with the increase in percentage of the suspended nanoparticles at any given Grashof number. An experimental study of the flow and heat transfer characteristics for copper-water based nanofluids through a straight tube with a constant heat flux at the wall was conducted by Xuan and Li (2003). Jou and Tzeng (2005) analyzed the heat transfer enhancement utilizing nanofluids in a two-dimensional enclosure for different pertinent parameters. Tiwari and Das (2007) have investigated the problem of heat transfer augmentation in a lid-driven square cavity filled with nanofluids. Oztop and Abu-Nada (2008) considered natural convection in partially heated enclosures having different aspect ratio and filled with nanofluid. Mahmoudi*et al*. (2010) considered numerically the effect of position of horizontal heat source on the left vertical wall of a cavity filled with Cu-water nanofluid. Their results showed that the presence of nanoparticles at low Ra was more pronounced; also when the heat source was located close to the top horizontal wall, nanofluid was more effective. Mansour *et al*. (2010) presented a numerical simulation on mixed convection flow in a square lid-driven cavity partially heated from below using a nanofluid. Talebi *et al*. (2010) investigated numerically the problem of mixed convection flows in a square lid-driven cavity utilizing nanofluid. The problem of natural convection cooling of a localized heat source at the bottom wall of an enclosure filled with Cu-water nanofluid for a variety of thermal boundary conditions at the sidewalls has been studied by Mansour *et al*. (2011). Ahmed *et al*. (2013) presented numerical solution of natural convection cooling of a localized heat source at the bottom wall of a triangular enclosure filled with Cu-water nanofluid. Nasrin and Alim (2014) performed the finite element simulation of heat transfer by various nanofluids containing double nanoparticles inside the riser pipe of a flat plate solar collector. The problem of laminar-forced convection nanofluids flow over a stretching surface at a porous surface has been numerically studied by Sheikholeslami and Ganji (2014). Arani *et al*. (2014) investigated the problem of natural convection of a nanofluid with variable properties in square cavity with different linear temperature distributions on side wall. Hayat *et al*. (2015) analyzed the boundary layer flow of power law nanofluid over a vertical stretching sheet.

On other hand, magnetic nanofluid is a magnetic colloidal suspension of carried liquid and magnetic nanoparticles. The advantage of magnetic nanofluid is that fluid flow and heat transfer can be controlled by external magnetic field, which makes it applicable in various fields such as electronic packing, thermal engineering and aerospace. Grosan *et al*. (2009) have studied the effects of magnetic field and internal heat generation on the free convection in a rectangular cavity filled with a porous medium. Ghasemi *et al*. (2011) considered the magnetic field effect on natural convection in a square enclosure filled by a nanofluid. They have used basic mixture model for calculation of effective electric conductivity of nanofluids. Their results showed that the effect of the solid volume fraction on the heat transfer rate strongly depends on the values of the Rayleigh and Hartman numbers. Nemati *et al*. (2012) studied numerically the effect of the magnetic field on natural convection of nanofluid by using Lattice Boltzmann model. Amir *et al.* (2013) have investigated the MHD natural convection and entropy generation in a trapezoidal enclosure using Cu- water nanofluid. Loganthan and Vimala (2015) analyzed the influence of the magnetic field on the forced convection boundary layer flow of a nanofluid over an exponentially stretching sheet, embedded in a thermally stratified medium.

Motivated by the investigations mentioned above, the aim of the present work is to consider numerical simulation for MHD natural convection in a square enclosure using nanofluid with the influence of thermal boundary conditions. Four cases were considered depends on different thermal conditions for the cavity walls.

## 2. MATHEMATICAL MODELING

Consider a steady natural convection flow inside a square cavity filled with nanofluid in the presence of magnetic field subjected to changeable thermal boundary conditions. The geometric and the Cartesian coordinate system are schematically shown in Fig. 1. In the present problem, the following assumptions have been made:

1. In the cavity, the bottom wall is kept to be adiabatic and the following four cases depends on different thermal conditions for the cavity walls as shown in Fig. 2, are considered: (a) Case 1: Right and left vertical walls cooled the top wall is assumed to be adiabatic.(b) Case 2: Top and left vertical walls cooled and the right wall adiabatic. (c) Case 3: Top wall and bottom half of the right and left vertical walls cooled and remaining parts of the vertical walls adiabatic. (d) Top and right vertical walls cooled and the left wall adiabatic.

**Table 1 Thermophysical properties of the base fluid and nanoparticles at $20^0$C**

| Property | water | Copper | Silver | Alumina | Titanum |
|---|---|---|---|---|---|
| $\rho$ | 997.1 | 8933 | 10500 | 3970 | 4250 |
| $C_p$ | 4179 | 385 | 235 | 765 | 686.2 |
| $K$ | 0.613 | 401 | 429 | 40 | 8.9538 |
| $\beta \times 10^{-5}$ | 21 | 1.67 | 1.89 | 0.85 | 0.9 |
| $\sigma$ | 0.05 | $5.96x10^7$ | $3.60x10^7$ | $1x10^{-10}$ | $1x10^{-12}$ |

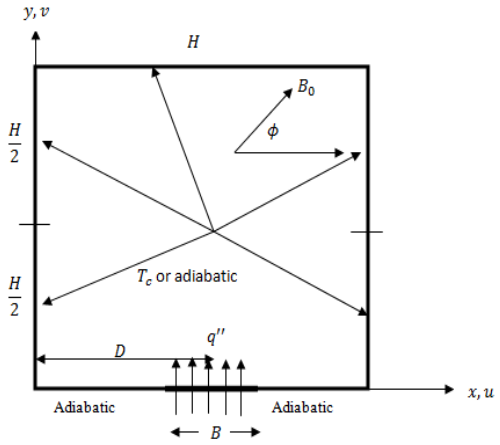


**Fig. 1. Sketch of the geometry and coordinate system of the cavity.**

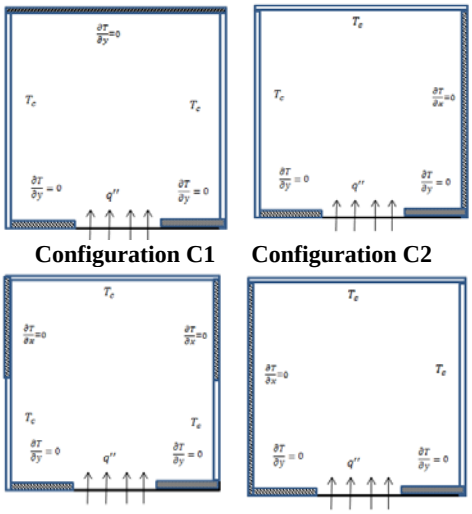

**Configuration C1** **Configuration C2**

**Configuration C3** **Configuration C4**

**Fig. 2. Thermal configurations of the cavity.**

2. A heat source is located on a part of the bottom wall and the other parts are thermally insulated.

3. It is also assumed that the enclosure is permeated by a uniform magnetic field, $B = B_x e_x + B_y e_y$ of constant magnitude $B = \left(B_x^2 + B_y^2\right)^{1/2}$, where Bx and By are space-independent, ex and ey are unit vectors in Cartesian coordinate system. $V = ue_x + ve_y$ is the field velocity. The orientation of the magnetic field forms an angle$\Phi$ with horizontal axis such as $\Phi = \tan B_y / B_x$ .

4. The base fluid (water) and the solid spherical nanoparticles (Copper (Cu), Silver (Ag), Alumina (Al2O3) and Titanium (TiO2) ) are in thermal equilibrium.

5. The thermo-physical properties of the nanofluid are assumed constant except for variation of the density which is determined based on Boussinesq approximation.

6. Table 1 presents the thermo-physical properties for the base fluid and the nanoparticles.

Under the above assumptions, the governing equations are (see Ahmed *et al.* (2013) and Aminossadatia and Ghasemi (2009));

$$\frac{\partial u}{\partial x} + \frac{\partial v}{\partial y} = 0 , \tag{1}$$

$$u\frac{\partial u}{\partial x} + v\frac{\partial u}{\partial y} = -\frac{1}{\rho_{nf}}\frac{\partial p}{\partial x} + \nu_{nf}\left(\frac{\partial^2 u}{\partial x^2} + \frac{\partial^2 u}{\partial y^2}\right) + \frac{\sigma_{nf} B_0^2}{\rho_{nf}}(v\sin\Phi\cos\Phi - u\sin^2\Phi) \tag{2}$$

$$u\frac{\partial v}{\partial x} + v\frac{\partial v}{\partial y} = -\frac{1}{\rho_{nf}}\frac{\partial p}{\partial y} + \nu_{nf}\left(\frac{\partial^2 v}{\partial x^2} + \frac{\partial^2 v}{\partial y^2}\right) + \frac{(\rho\beta)_{nf}}{\rho_{nf}} g\,(T - T_c) + \frac{\sigma_{nf} B_0^2}{\rho_{nf}}(u\sin\Phi\cos\Phi - v\cos^2\Phi) \tag{3}$$

$$u\frac{\partial T}{\partial x} + v\frac{\partial T}{\partial y} = \alpha_{nf}\left(\frac{\partial^2 T}{\partial x^2} + \frac{\partial^2 T}{\partial y^2}\right) . \tag{4}$$

Where $x$ and $y$ are Cartesian coordinates measured along the horizontal and vertical walls of the cavity respectively, $u$ and $v$ are the velocity components along the $x$- and $y$- axes respectively, T is the fluid temperature, p is the fluid pressure, $g$ is the gravity acceleration, $\Phi$ is the inclination angle. Numerous formulations for the thermo-physical properties of nanofluids are proposed in the literature. In the present study, we are adopting the relations which depend on thenanoparticles volume fraction only and which were proven and used in many previous studies (Aminossadatia and Ghasemi (2009) and Brinkman (1952)) as follows:

The effective density of the nanofluid is given as:

$$\rho_{nf} = (1-\phi)\rho_f + \phi\rho_p, \tag{5}$$

Where $\varphi$ is the solid volume fraction of the nanofluid, $\rho_f$ and $\rho_p$ are the densities of the fluid and of the solid fractions respectively, and the heat capacitance of the nanofluid given is by Khanafer*et al*. (2003) as;

$$(\rho c_p)_{nf} = (1-\varphi)(\rho c_p)_f + \varphi(\rho c_p)_p. \tag{6}$$

The thermal expansion coefficient of the nanofluid can be determined by:

$$(\rho\beta)_{nf} = (1-\varphi)(\rho\beta)_f + \varphi(\rho\beta)_p \tag{7}$$

Where $\beta_f$ and $\beta_p$ are the coefficients of thermal expansion of the fluid and of the solid fractions respectively. Thermal diffusivity, $\alpha_{nf}$ of the nanofluid is defined by Oztop and Abu-Nada (2008) as:

$$\alpha_{nf} = \frac{k_{nf}}{(\rho c_p)_{nf}} \tag{8}$$

In Eq. (8), $k_{nf}$ is the thermal conductivity of the nanofluid which estimated in the present study according to Yu and Choi model (2003) that can be considered an updated model of Maxwell-Garnetts model (Maxwell (1904)),:

$$\frac{k_{nf}}{k_f} = \frac{(k_p + 2k_f) - 2\varphi(1+\zeta)^3(k_f - k_p)}{(k_p + 2k_f) + \varphi(1+\zeta)^3(k_f - kp)}. \tag{9}$$

where $\zeta$ in Eq. (9) represents the ratio of nanolayer thickness to nanoparticle radius and thereby accounts for the size dependent nature of thermal conductivity of nanofluids. This model attributes the enhanced thermal conductivity of nanofluid to the solidlike layering of liquid at nanoparticle/base fluid interface.Here, $\zeta$ is set equal to 0.1, which implies a nanolayer thickness of 1 nm.

The effective dynamic viscosity of the nanofluid based on the Brinkman model [20] is given by

$$\mu_{nf} = \frac{\mu_f}{(1-\varphi)^{2.5}}, \tag{10}$$

Where $\mu_f$is the viscosity of the fluid fraction and the effective electrical conductivity of nanofluid was presented by Maxwell (1904) as;

$$\frac{\sigma_{nf}}{\sigma_f} = 1 + \frac{3(\gamma-1)\varphi}{(\gamma+2) - (\gamma-1)\varphi} \tag{11}$$

where $\gamma = \frac{\sigma_p}{\sigma_f}$.

Introducing the following dimensionless set:

$$\begin{aligned} &X = \frac{x}{H}, Y = \frac{y}{H}, U = \frac{uH}{\alpha_f}, V = \frac{vH}{\alpha_f}, \\ &P = \frac{pH^2}{\rho_{nf}\alpha_f^2}, \theta = -\frac{(T - T_c)}{Hq''}.\frac{k_f}{k_{nf}} \end{aligned} \tag{12}$$

intoEqs. (1)-(4) yields the following dimensionless equations:

$$\frac{\partial U}{\partial X} + \frac{\partial V}{\partial Y} = 0, \tag{13}$$

$$\begin{aligned} &U\frac{\partial U}{\partial X} + V\frac{\partial U}{\partial Y} = -\frac{\partial P}{\partial X} \\ &+ \frac{\mu_{nf}}{\rho_{nf}\alpha_f}\left(\frac{\partial^2 U}{\partial X^2} + \frac{\partial^2 U}{\partial Y^2}\right) + \\ &Ha^2.\Pr.\frac{\sigma_{nf}}{\sigma_f}.\frac{\rho_f}{\rho_{nf}}(V\sin\Phi\cos\Phi - U\sin^2\Phi) \end{aligned} \tag{14}$$

$$\begin{aligned} &U\frac{\partial V}{\partial X} + V\frac{\partial V}{\partial Y} = -\frac{\partial P}{\partial Y} + \frac{\mu_{nf}}{\rho_{nf}\alpha_f}\left(\frac{\partial^2 V}{\partial X^2} + \frac{\partial^2 V}{\partial Y^2}\right) \\ &+ \frac{(\rho\beta)_{nf}}{\rho_{nf}\beta_f} Ra\Pr\theta + \\ &Ha^2\Pr\frac{\sigma_{nf}}{\sigma_f}\frac{\beta_f}{\rho_{nf}}(U\sin\Phi\cos\Phi - V\cos^2\Phi), \end{aligned} \tag{15}$$

$$U\frac{\partial\theta}{\partial X} + V\frac{\partial\theta}{\partial Y} = \frac{\alpha_{nf}}{\alpha_f}\left(\frac{\partial^2\theta}{\partial X^2} + \frac{\partial^2\theta}{\partial Y^2}\right) \tag{16}$$

Where

$\Pr = \frac{\nu_f}{\alpha_f}, Ra = \frac{g\beta_f\,\Delta T\,H^3}{\nu_f\,\alpha_f}, Ha = B_0 H\sqrt{\frac{\sigma_f}{\mu_f}}$ are respectively the Prandtl number, the Rayleigh number and the Hartman number.

The enclosure boundary conditions consist of no-slip and no-penetraction walls, i.e. $u = v = 0$ on all four walls. The thermal boundary conditions assumed are $\theta = 0$ or $\partial\theta/\partial n = 0$ at any cooled or adiabatic sidewalls, respectively. Here, $n$ is the unit normal to the boundary surface. On the bottom wall the boundary conditions are as follows:

$$\frac{\partial\theta}{\partial Y} = \begin{cases} 0 & for \quad 0 \le X \le D - B/2 \\ -\frac{k_{nf}}{k_f} & for \quad D - B/2 \le X \le D + B/2 \\ 0 & for \quad D + B/2 \prec X \prec 1 \end{cases} \tag{17}$$

The local Nusselt number is defined as:

$$Nu_s = \frac{1}{\theta_s(X)} \tag{18}$$

And the average Nusselt number is defined as:

$$Nu_m = \frac{1}{B}\int_{D-0.5*B}^{D+0.5*B} Nu_s\,dX \tag{19}$$

**Table 2 Numerical comparisons for various Ra at Ha=0**

| *Ra* | Grosan *et al*. (2009) | | Haajizadeh *et al*. (1984). | | Present method | |
|---|---|---|---|---|---|---|
| | $\psi_{max}$ | $\theta_{max}$ | $\psi_{max}$ | $\theta_{max}$ | $\psi_{max}$ | $\theta_{max}$ |
| 10 | 0.079 | 0.127 | 0.078 | 0.130 | 0.0799 | 0.1272 |
| $10^3$ | 4.833 | 0.116 | 4.880 | 0.118 | 4.8266 | 0.117 |

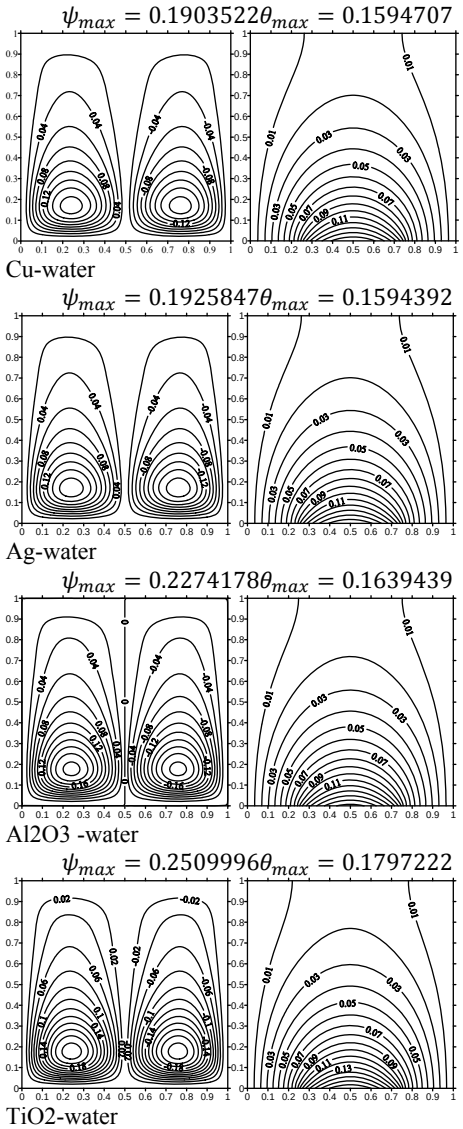


**Fig. 3. Streamlines (left) and isothermal (right) for different nanofluids and C1at** $Ra = 10^5, Ha = 50, D = 0.5, B = 0.5, \phi = 0.05, \Phi = 0^0$ $\boldsymbol{\psi_{max} = 0.1903522\theta_{max} = 0.1594707}$.

## 3. NUMERICAL SECTION

In the present study, the iterative finite difference method is used to solve the dimensionless governing equations (13)-(16) subject to their corresponding boundary conditions given in Eq. (17). Approximation of convective terms is based on an second order upwind finite differencing scheme, which correctly represent the directional influence of a disturbance. A uniform grid resolution of $81 \times 81$ is found to be suitable. As convergence criteria, the dependent variables were calculated iteratively until the relative difference between the current and the previous iterations reaches $10^{-5}$.In order to verify the accuracy of the present numerical study, the present numerical model was validated against the results obtained by Grosan *et al*. (2009) and Haajizadeh *et al*. (1984) in special cases of the current investigation. These comparisons are presented in table 2. An excellent agreement was found between the present results and the results obtained by Grosan *et al*. (2009) and Haajizadeh *et al*. (1984). Therfore, we are confident that the results presented in this paper are very accurate.

## 4. RESULTS AND DISCUSSION

The physical effects of the governing parameter are discussed in this section. At the outset, we should refer to that wide ranges of the governing parameters are considered, namely, Hartmann number ($0 \leq \mathrm{Ha} \leq 50$), the heat source length ($0.2 \leq \mathrm{B} \leq 0.8$), different locations of the heat source ($0.3 \leq \mathrm{D} \leq 0.7$), nanoparticles volume fraction ($0 \leq \emptyset \leq 0.1$) and Rayleigh number ($10^3 \leq \mathrm{Ra} \leq 10^6$) . In all the obtained results water is considered to be a base fluid with $\mathrm{Pr} = 6.2$.

Fig. 3 Shows the streamlines and isotherms contours for different nanoparticles for configuration C1. It is observed that, among all nanoparticles, $TiO_2$-water nanofluid gives a good convection and Cu-water nanofluid has a lowest one. This behavior is due to the values of the thermal conductivity presented in table 1. From this table, one can found that Cu has the lowest thermal conductivity. The effects of the thermal boundary layer are represented, here, by changing the thermal conditions of the cavity walls. It is found from Fig. 4 which displays this effects that, For C1 (the top wall is assumed to be adiabatic and the vertical walls are cooled), there are a symmetrical flow of the nanofluid about the vertical center line of the enclosure ($Y = 0.5$). This asymmetry disappears when we change the right wall to become thermally insulated and the top and left walls to be cooled (C2). The fluid flow in this case represented by one anticlockwise circular cell occupied the whole

enclosure and the isotherms concentrate in the right half of the cavity. In C3, the fluid motion is represented by two clockwise and anticlockwise eddies inside the enclosure. The mean reason for the formulation of this behavior is due to the symmetrical of the thermal condition of the vertical walls. The isotherms lines concentrate in the bottom half of the cavity near the heat source indicating large temperature differences in the enclosure. There is a fully opposite behavior of C2 can be seen when C4 is considered. The reason for that are the thermal conditions for C4 which is inverse to C2. In this case the streamlines show a large clockwise eddy appears in the right half of the enclosure. The isotherms lines gather in the left half of the cavity near the left vertical wall indicating a high buoyancy force in the right half of the cavity. All these behaviors are presented in Fig. 4 at $Ra = 10^5, Ha = 50, D = 0.5, B = 0.5, \phi = 0.05, \Phi = 0^0$ .

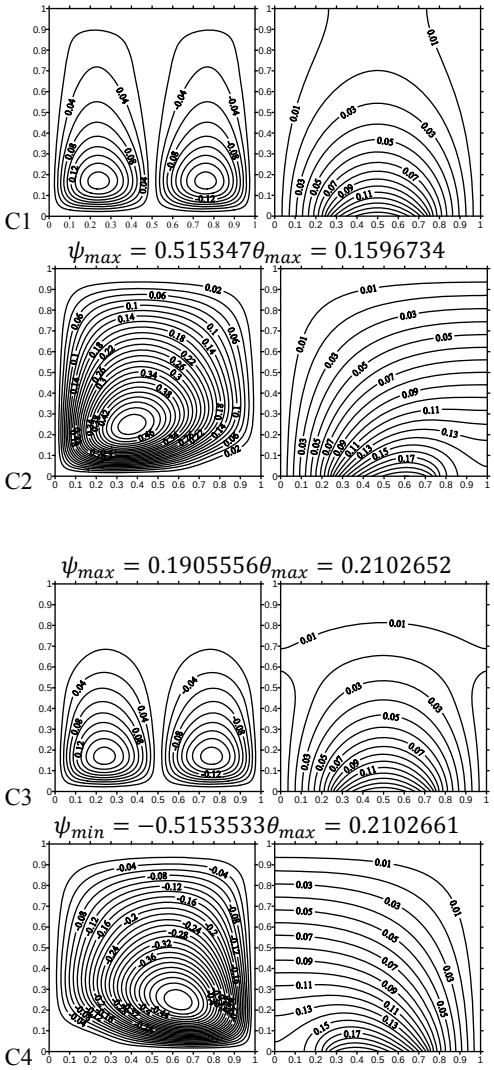


**Fig. 4. Streamlines (left) and Isothermal (right) for Cu-water nanofluid for different configurations at**

$Ra = 10^5, Ha = 50, D = 0.5, B = 0.5, \phi = 0.05, \Phi = 0^0$

$. \psi_{max} = 2.994272 \theta_{max} = 0.1456744$

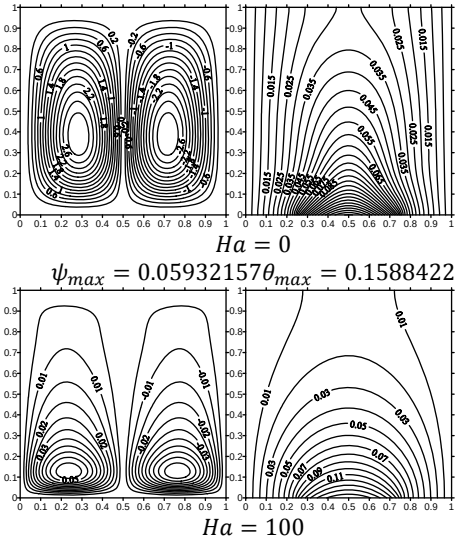


**Fig. 5. Streamlines (left) and isothermal (right) for Cu-water nanofluid and C1 at**

$Ra = 10^5, D = 0.5, B = 0.5, \phi = 0.05, \Phi = 0^0$ .

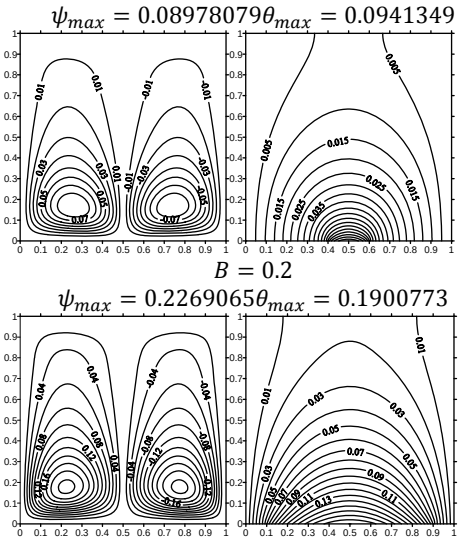


**Fig. 6. Streamlines (left) and isothermal (right) for Cu-water and C1 at**

$Ra = 10^5, Ha = 50, D = 0.5, \phi = 0.05, \Phi = 0^0$ .

The effects of the Hartmann number Ha on the streamlines and isotherms contours for Cu-water nanofluid for C1 is presented in Fig. 5. It is clear that, in the absence of the magnetic force (Ha=0), a good convection is obtained and the fluid flows strongly inside the cavity. Also, the isotherms tend to gather beside the vertical walls. The activity of the fluid can be observed from the maximum value of stream function which recorded $\psi_{max} = 2.994272$ at Ha =0. Also, the maximum value of the temperature recorded$\theta_{max} = 0.1456744$. However, this behavior is damped when we consider$Ha = 100$. The maximum value of stream function decreases to become $\psi_{max} = 0.05932157$, whereas the maximum value of temperature increases to record $\theta_{max} = 0.1588422$. The Physical explanation for this

behavior is due to Lorentz force resulting from the presence of magnetic field, which suppresses the motion.

Figure 6. displays the effect of the heat source length B on the streamlines and isotherms for C2 for Cu-water nanofluid. It is noted that when the heat source is short (B = 0.2) a weak convective is obtained and the fluid flows, in this case, in form of two symmetrical vortices with $\psi_{\max} = 0.08978079$ inside the enclosure and this behavior is due to symmetrical thermal condition of the vertical walls. Increasing B to 0.8 leads to increase natural convection and accordingly, the fluid become more activity. It is also normal that, when B increases, the maximum value of the temperature increases. This behavior can be attributed to the total heat generation obtained from the heat source that increases as B increases.

Fig. 7 shows the effects of the different locations of the heat source D on the contours of streamlines and isotherms for Cu-water nanofluid for C3 at $Ra = 10^5, Ha = 50, B = 0.5, \phi = 0.05, \Phi = 0^0$. It is observed that, when $D = 0.3$ (the heat source located at the left half of the bottom wall), the fluid motion concentrates in the right hand side of the cavity forming large clockwise egg-shape cell in the right half of the cavity and small anticlockwise eddy in the left half. The isotherms lines gather in the left half of the cavity where the heat source is located indicating large temperature difference in the right half of the cavity. At D=0.7, the fully inverse behavior is occurred for both streamlines and isotherms.

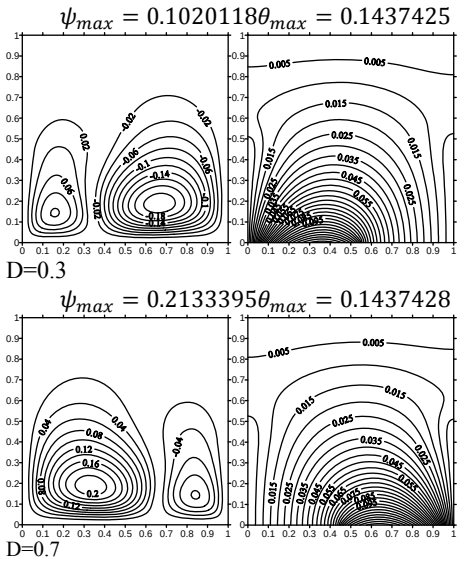


**Fig. 7. Streamlines (left) and isothermal (right) for Cu-water and C3 at** $Ra = 10^5, Ha = 50, B = 0.5, \phi = 0.05, \Phi = 0^0$.

On the other hand, adding the nanoparticles to the base fluid decay its movement. This can be noted from Fig. 8 which shows the streamlines and isotherms contours for Cu-water nanofluid for C4 at $\phi = 0$ and $\phi = 0.1$. The maximum temperature, also, decreases form $\theta_{max} = 0.3744806$ to $\theta_{max} = 0.1058501$as $\phi$ from 0% to 10%. The reason for that is the fluid become mores viscose by adding the nanoparticles accordingly the natural convection decreases.

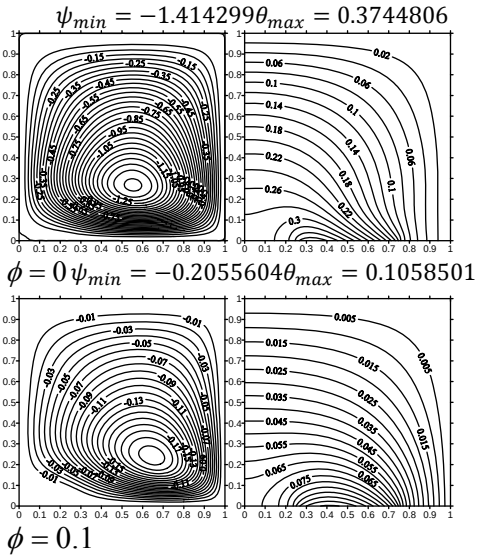


**Fig. 8. Streamlines (left) and isothermal (right) for Cu-water and C4 at** $Ra = 10^5, Ha = 50,$ $B = 0.5, D = 0.5, \Phi = 0^0$.

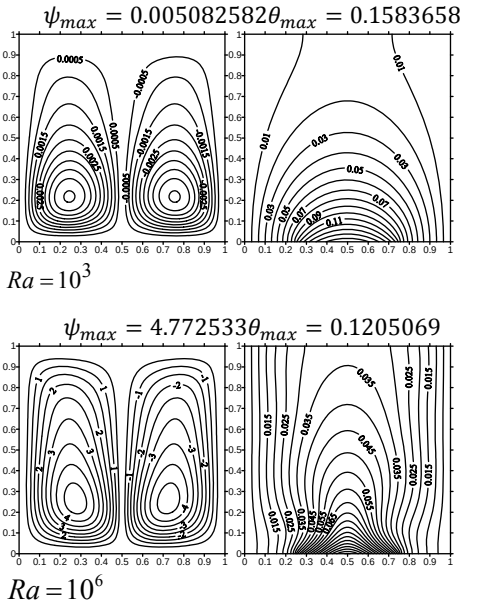


**Fig. 9. Streamlines(left) and isothermal (right) for Cu-water and C1 at** $Ha = 25, B = 0.5,$ $D = 0.5, \phi = 0.05, \Phi = 0^0$

There are clear enhancements in the fluid motion and the maximum temperature can be found by increasing Ra from $10^3$to $10^6$. In this case, the nanofluid flows strongly and the isotherms line amassing beside the vertical walls. The reason for that is due to buoyancy force which controlling the natural convection in such type of problems. This behavior is presented in Fig.9 for Cu-water and C1

at $Ha = 50, B = 0.5,\ D = 0.5, \phi = 0.05, \Phi = 0^0$ .

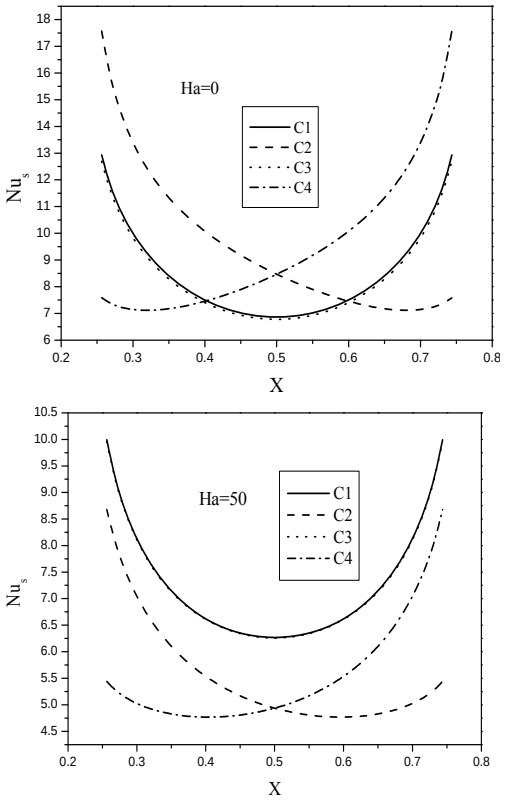


**Fig. 10. Effects of Ha on the profiles of the local Nusselt number along the heat source for Cu-water at**

$Ra = 10^5, D = 0.5, B = 0.5, \varphi = 0.05, \Phi = 90^0$ .

Fig. 10 shows that the local Nusselt number decreases as $Ha$ increases. Also, among all configurations, C1 has the higher Nusselt number at $Ha = 50$. However, at any value of $Ha$, C3 has local Nusselt number behavior that converges to the local Nusselt number behavior obtained from C1.

Fig. 11 shows that $Nu_s$ decreases for all configurations as $B$ increases and at any value of $B$, C1 has the highest rate of heat transfer. Fig. 12 shows that, at D=0.3, $Nu_s$ takes its maximum at the beginning of the heat source and gets its minimum at the end of the heat source. This for C1, C2 and C3, while for C4, the inverse behavior is occurred. At D=0.7, $Nu_s$ takes the opposite behavior. Fig. 13 shows a slightly enhancement in the rate of heat transfer can be obtained by increasing $\phi$ from 0% to 10%. The increase in Ra, also, leads to increase the local Nusselt number at the heat source. This can be observed clearly from Fig. 14. Figs. 15 and 16 show the effects of $Ha, B$ and $\Phi$ on the average Nusselt number $Nu_m$. It is found that $Nu_m$decreases by increase either B or Ha. For C1 and C3 the increase in $\Phi$ leads to increase the average Nusselt number whereas, for other configurations $\Phi$ has not a clear effect on $Nu_m$.. For all cases, the increase in $Ra$ gives an excellent support for $Nu_m$, this can be observed from Figs. 17 and 18. Also, $TiO_2$ has the lowest rate of heat transfer.

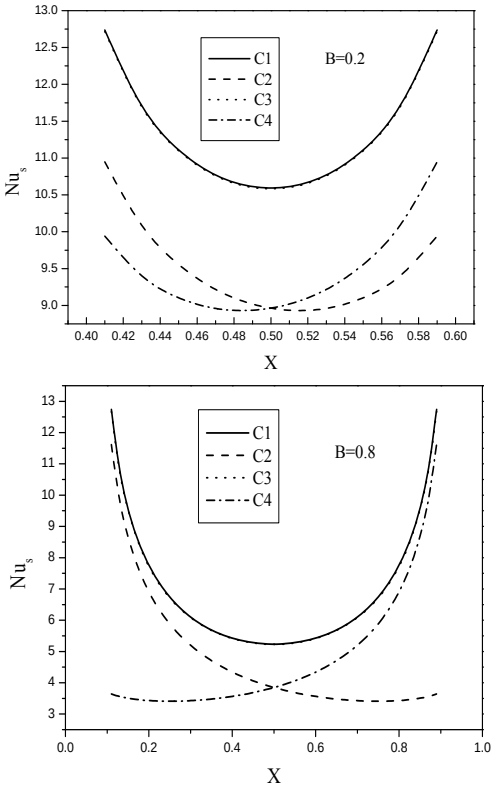


**Fig. 11. Effects of B on the profiles of the local Nusselt number along the heat source for Cu-water at**

$Ha = 50, Ra = 10^5, D = 0.5, \varphi = 0.05, \Phi = 90^0$ .

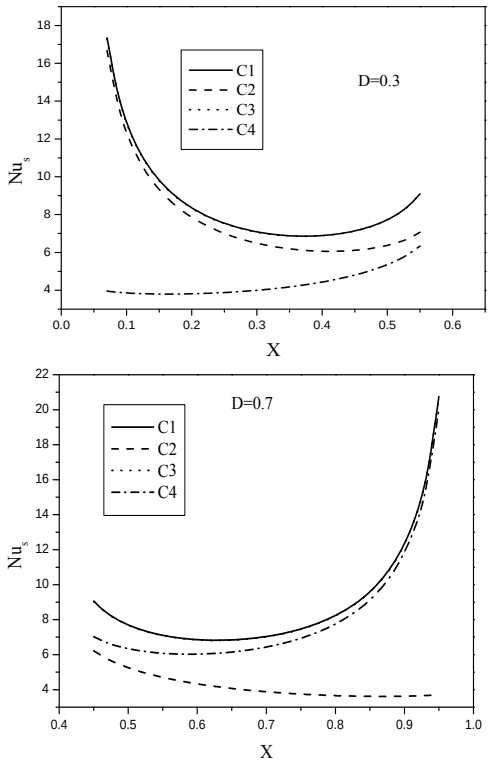


**Fig. 12. Effects of D on the profiles of the local Nusselt number along the heat source for Cu-water at**

$Ha = 50, Ra = 10^5, B = 0.5, \varphi = 0.05, \Phi = 90^0$ .

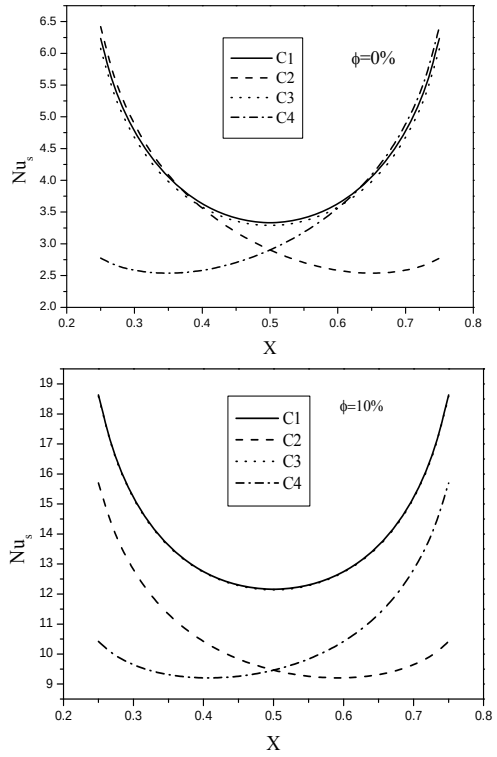


**Fig. 13. Effects of $\phi$ on the profiles of the local Nusselt number along the heat source for Cu-water at**

$Ha = 50, Ra = 10^5, B = 0.5, D = 0.5, \Phi = 90^0$.

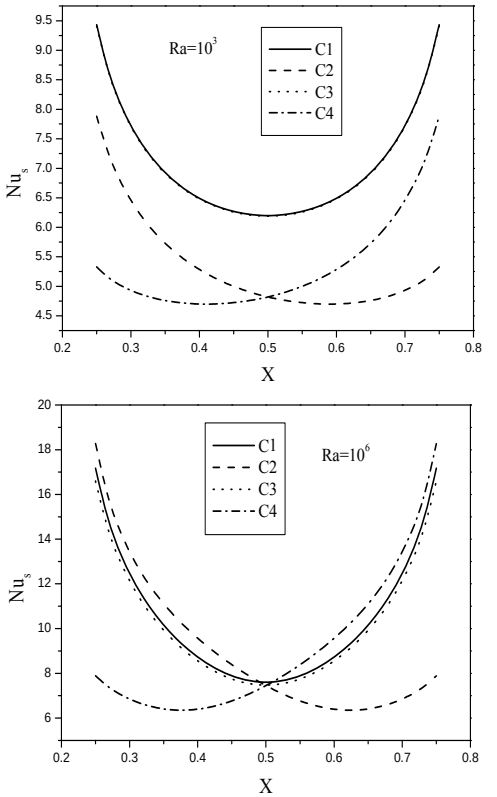


**Fig 14. Effects of Ra on the profiles of the local Nusselt number along the heat source for Cu-water at**

$Ha = 50, B = 0.5, D = 0.5, \varphi = 0.05, \Phi = 90^0$.

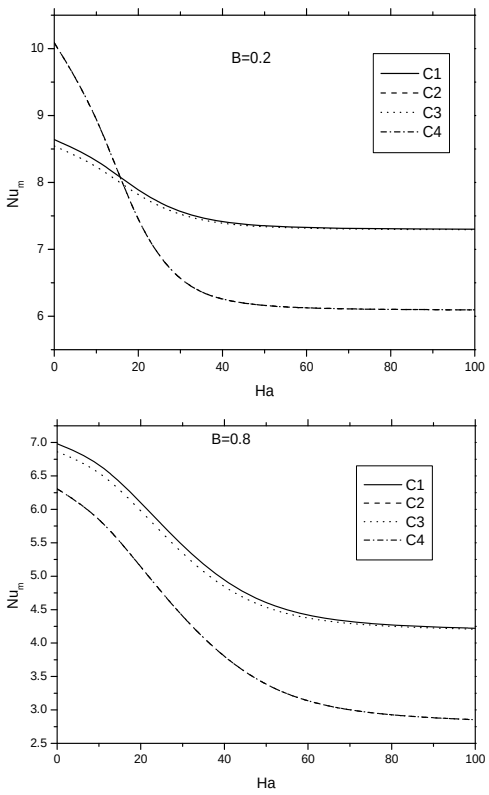


**Fig. 15. Average of Nusselt number for different values of B for Cu-water at.**

$Ra = 10^5, D = 0.5, \phi = 0.05, \Phi = 90^0$.

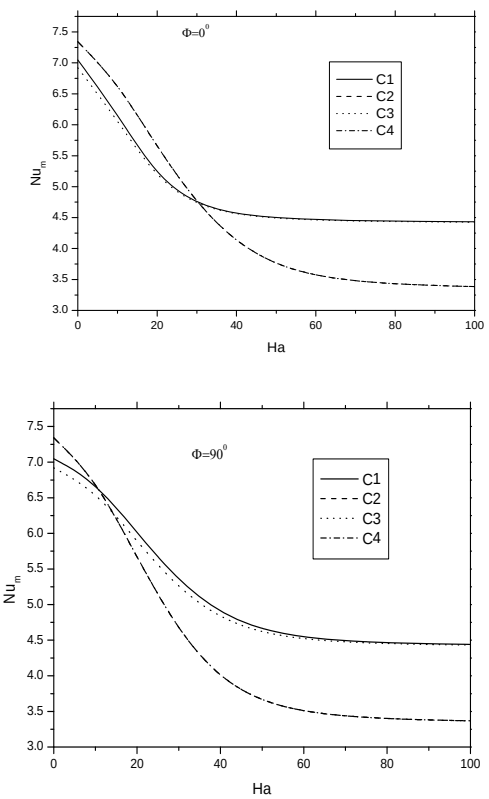


**Fig. 16. Average Nusselt number for different values of** $Ra = 10^5, B = 0.5, D = 0.5, \phi = 0.05$.

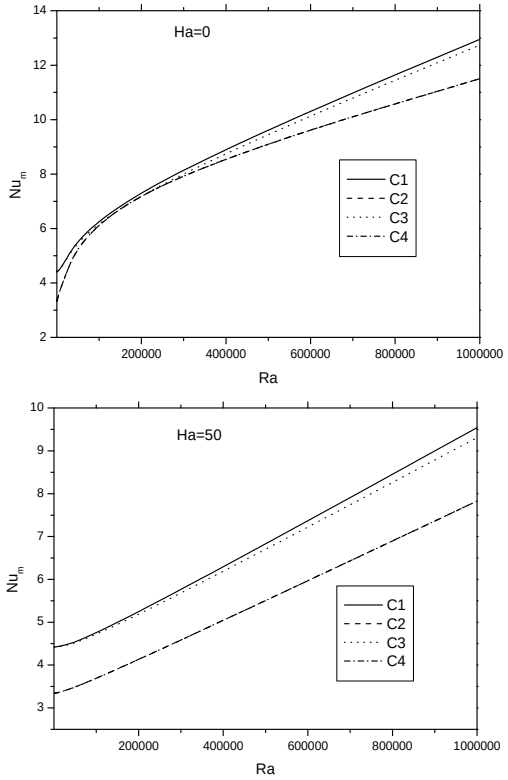


**Fig. 17. Average of Nusselt number at** $B = 0.5, D = 0.5, \phi = 0.05, \Phi = 90^0$.

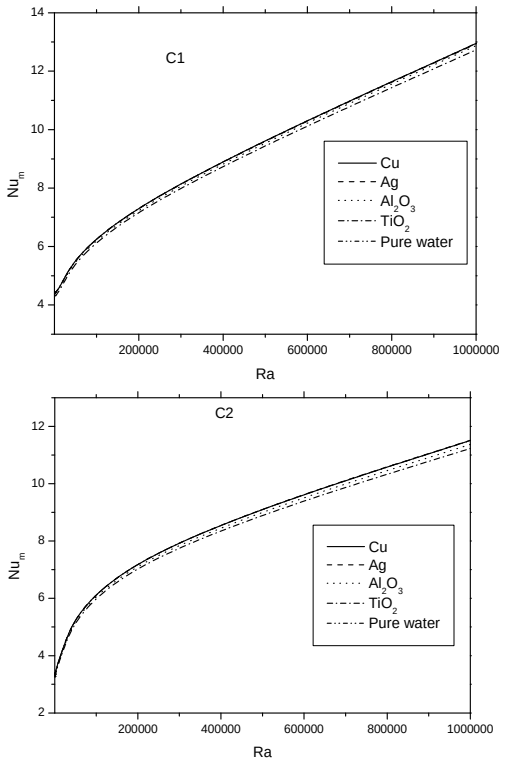


**Fig. 18. Average of Nusselt number at** $Ha = 50, B = 0.5, D = 0.5, \phi = 0.05, \Phi = 90^0$.

## 5. CONCLUSIONS

This paper presents a numerical simulation for MHD natural convection in a square enclosure using nanofluid with the influence of thermal boundary conditions. Four cases were considered depends on different thermal conditions for the cavity walls. Finite difference method was used to solve the dimensionless form of the boundary condition. Comparisons with previously published works were formulated and found to be in a very good agreement. From the current investigation, it can be concluded that;

1. The fluid flow is symmetric around a vertical centerline in C1 and C3 and this asymmetry disappears for the other cases.
2. Considering the top is adiabatic helps to transfer temperature all over the cavity.
3. The relation between average $Nu_m$ and Ha is decreasing globally.
4. The relation of average Nu and Ra is globally increasing and linear.
5. The presence of the nanoparticle in the base fluid gives a good enhancement of the heat transfer rate.
6. Increasing the heat source length leads to a decrease the average Nusselt number.
7. For C1, as the magnetic field inclination angle increases, the convection regime has been enhanced because the magnetic field mitigates its effect on buoyancy force.

## REFERENCES

AbbasianArani, A. A., M. Mahmoodi and S. MazroueiSebdani (2014). On the cooling process of nanofluid in a square enclosure with linear temperature distribution on left wall. *Journal of Applied Fluid Mechanics*7(4), 591-601.

Ahmed, S. E., A. M. Rashad and R. S. R. Gorla (2013). Natural convection in a triangular enclosure filled with a porous medium saturated with Cu-water nanofluid. *Journal of Thermophysics and Heat Transfer* 27(4), 700-706.

Aminossadatia, S. M. and B. Ghasemi (2009). Natural convection cooling of a localized heat source at the bottom of a nanofluid-filled enclosure. *Europian Journal of Mechanics B/Fluid 28, 630-640*.

Brinkman, H. C. (1952). The viscosity of concentrated suspensions and solution. *Journal of Chemical Physics.* 20, 571-581.

Choi, S. U. S. (1995). Enhancing thermal conductivity of fluids with nano particles. *ASME Fluids Eng. Div. 231, 99-105.*

Eastman, J. A., S. U. S. Choi, S. Li, W. Yu and L. J. Thompson (2001). Anomalously increased effective thermal conductivities of ethylene glycol-based nanofluids containing copper nanoparticles. *Applied Physics Letters 78(6), 718-720.*

Ghasemi B, S. M. Aminossadati and A. Raisi (2011). Magnetic field effect on natural

convection in a nanofluid-filled square enclosure. *International Journal of Thermal Sciences 50,1748–56*.

Grosan, T., C. Revnic, I. Pop and D. B. Ingham (2009). Magnetic field and internal heat generation effects on the free convection in a rectangular cavity filled with a porous medium. *International Journal of Heat Mass Transfer 52, 1525-1533.*

Haajizadeh, M., A. F. Ozguc and C. L. Tien (1984). Natural convection in a vertical porous enclosure with internal heat generation. *International Journal of Heat Mass Transfer 27, 1893-190*.

Hayat, T., M. Hussain, A. Alsaedi, S. A. Shehzad and G. Q. Chen (2015). Flow of Power-Law Nanofluid over a Stretching Surface with Newtonian Heating. *Journal of Applied Fluid Mechanics 8(2), 273-280.*

Jana, S., A. Salehi-Khojin and W. H. Zhong (2007). Enhancement of fluid thermal conductivity by the addition of single and hybrid nanoadditives. *ThermochimActa 462(1-2), 45-55.*

Khanafer, K., K. Vafai and M. Lightstone (2003). Buoyancy-driven heat transfer enhancement in a two-dimensional enclosure utilizing nanofluids. *International Journal of Heat and Mass Transfer 46, 3639-3653*.

Loganthan, P. and C. Vimala (2015). MHD flow of nanofluids over an exponentially stretching sheet embedded in a stratified medium with suction and radiation effects. *Journal of Applied Fluid Mechanics 8(1), 85-93.*

Mahmoudi, A. H., I. Pop, M. Shhi and F. Talebi (2013). MHD natural convection and entropy generation in a trapezoidal enclosure using Cu-water nanofluid. *Computers and Fluids 27, 46-62.*

Mahmoudi, A. H, M. Shahi, A. Raouf and A. Ghasemian (2010). Numerical study of natural convection cooling of horizontal heat source mounted in a square cavity filled with nanofluid. *International Communication in Heat and Mass Transfer 37, 1135-1141*.

Mansour, M. A., R. A. Mohamed and S. E. Ahmed (2011). Natural convection cooling of a heat source embedded on the bottom of an enclosure filled with Cu-water nanofluid: effects of various thermal boundary conditions. *Heat and Mass Transfer 47, 1479-1490.*

Mansour, M. A., R. A. Mohamed, M. M. Abd-Elaziz and S. E. Ahmed (2010). Numerical simulation of mixed convection flows in a square lid-driven cavity partially heated from below using nanofluid. International *Communication in Heat and Mass Transfer 37, 1504-1512.*

Maxwell, J. (1904*). A Treatise on Electricity and Magnetism.* Second edn., Oxford University Press, Cambridge, UK.

Nasrin, R. and M. A. Alim (2014). Finite element simulation of forced convection in a flat plate solar collector: influence of nanofluid with double nanoparticles. *Journal of Applied Fluid Mechanics 7(3), 543-556.*

Nemati, H., M. Farhadi,K. Sedighi, H. R. Ashorynejad and E. Fattahi (2012). Magnetic field effects on natural convection flow of nanofluid in a rectangular cavity using the Lattice Boltzmann model. SciIranica, in press.

Oztop, H. F. and E. Abu-Nada (2008). Numerical study of natural convection in partially heated rectangular enclosure filled with nanofluids. *International Journal of Heat and Fluid Flow 29(5), 1326-1336.*

Sheikholeslami, M. and D. D. Ganji (2014). Heated permeable stretching surface in a porous medium using nanofluids. *Journal of Applied Fluid Mechanics 7(3), 535-542*.

Talebi, F., A. H. Mahmoudi and M. Shahi (2010). Numerical study of mixed convection flows in a square lid-driven cavity utilizing nanofluid. *International Communications in Heat and Mass Transfer 37, 79-90.*

Tiwari, R. K. and M. K. Das (2007). Heat transfer augmentation in a two-sided lid-driven differentially heated square cavity utilizing nanofluids. *International Journal of Heat and Mass Transfer 50, 2002-2007.*

Tzeng, S. C., C. W. Lin and K. D. Huang (2005). Heat transfer enhancement of nanofluids in rotary blade coupling of four-wheel-drive vehicles. *ActaMechenica 179, 11-23*.

Xie, H. Q., H. Lee, W. Youn and M. Choi (2003). Nanofluids containing multi walled carbon nanotubes and their enhanced thermal conductivities. *Journal of Applied Physics 94(8), 4967-4971.*

Xuan,Y. and Q. Li (2003). Investigation on convective heat transfer and flow features of nanofluids. *ASME Journal of Heat Transfer 125, 151-156.*

Yu, W., and S. Choi (2003). The role of interfacial layers in the enhanced thermal conductivity of nanofluids: A renovated Maxwell model. *Journal of Nanoparticle Research 5(1–2), 167–171*.